

Structures buckling under tensile dead load

D. Zaccaria⁽¹⁾, D. Bigoni⁽²⁾, G. Noselli⁽²⁾ and D. Misseroni⁽²⁾

⁽¹⁾*Department of Civil and Environmental Engineering, University of Trieste
piazzale Europa 1, Trieste, Italy*

⁽²⁾*Department of Mechanical and Structural Engineering, University of Trento
via Mesiano 77, Trento, Italy*

Abstract

Some 250 years after the systematic experiments by Musschenbroek and their rationalization by Euler, for the first time we show that it is possible to design structures (i.e. mechanical systems whose elements are governed by the equation of the elastica) exhibiting bifurcation and instability ('buckling') under tensile load of constant direction and point of application ('dead'). We show both theoretically and experimentally that the behaviour is possible in elementary structures with a single degree of freedom and in more complex mechanical systems, as related to the presence of a structural junction, called 'slider', allowing only relative transversal displacement between the connected elements. In continuous systems where the slider connects two elastic thin rods, bifurcation occurs both in tension and compression and is governed by the equation of the elastica, employed here for tensile loading, so that the deformed rods take the form of the capillary curve in a liquid, which is in fact governed by the equation of the elastica under tension. Since axial load in structural elements deeply influences dynamics, our results may provide application to innovative actuators for mechanical wave control, moreover, they open a new perspective in the understanding of failure within structural elements.

Keywords: Elastica, bifurcation, instability under tension

1 Introduction

Buckling of a straight elastic column subject to *compressive* end thrust occurs at a critical load for which the straight configuration of the column becomes unstable and simultaneously

²Corresponding author: Davide Bigoni - fax: +39 0461 882599; tel.: +39 0461 882507; website: <http://www.ing.unitn.it/~bigoni/>; e-mail: bigoni@ing.unitn.it.

ceases to be the unique solution of the elastic problem (so that instability and bifurcation are concomitant phenomena). Buckling is known from ancient times: it has been experimentally investigated in a systematic way by Pieter van Musschenbroek (1692-1761) and mathematically solved by Leonhard Euler (1707-1783), who derived the differential equation governing the behaviour of a thin elastic rod suffering a large bending, the so-called ‘elastica’ (see Love, 1927).

Through centuries, engineers have experimented and calculated complex structures, such as frames, plates and cylinders, manifesting instabilities and bifurcations of various forms (Timoshenko and Gere, 1961), so that certain instabilities have been found involving tensile loads. For instance, there are examples classified by Ziegler (1977) as ‘buckling by tension’ where a tensile loading is applied to a system in which a compressed member is always present, so that they do not represent true bifurcations under tensile loads. Other examples given by Gajewski and Palej (1974) are all related to the complex *live* (as opposed to ‘dead’) loading system, for instance, loading through a vessel filled with a liquid, so that Zyczkowski (1991) points out that ‘With Eulerian behaviour of loading (materially fixed point of application, direction fixed in space), the bar cannot lose stability at all [...]’. Note finally that necking of a circular bar represents a bifurcation of a material element under tension, not of a structure.

It can be concluded that until now *structures made up of line elements (each governed by the equation of the elastica) exhibiting bifurcation and instability under tensile load of fixed direction and point of application (in other words ‘dead’) have never been found*, so that the word ‘buckling’ is commonly associated to compressive loads.

In the present article we show that:

- simple structures can be designed evidencing bifurcation (buckling) and instability under tensile dead loading;
- the deformed shapes of these structures can be calculated using the equation of the elastica, but under tension, so that the deflection of the rod is identical to the shape of a capillary curve in a liquid, which is governed by the same equation, see Fig. 1 and Sections 3.2 and 4;
- experiments show that elastic structures buckling under tension can be realized in practice and that they closely follow theory predictions, Sections 2 and 4.

The above findings are complemented by a series of minor new results for which our system behaves differently from other systems made up of elastic rods, but with the usual end conditions. First, our system evidences load decrease with increase of axial displacement (the so-called ‘softening’), second, the bifurcated paths involving relative displacement at the slider terminate at an unloaded limit configuration, for both tension and compression.

We will see that the above results follow from a novel use of a junction between mechanical parts, namely, a *slider* or, in other words, a connection allowing only relative sliding (transverse displacement) between the connected pieces and therefore constraining the relative rotation and axial displacement to remain null.

Vibrations of structures are deeply influenced by axial load, so that the speed of flexural waves vanishes at bifurcation (Bigoni et al. 2008; Gei et al. 2009), a feature also evidenced

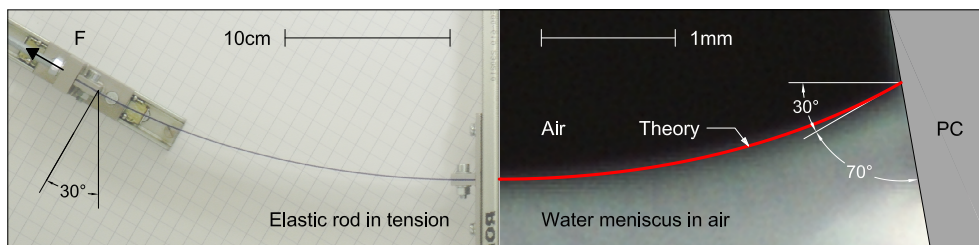


Fig. 1: Analogy between an elastic rod buckled under tensile force (left) and a water meniscus in a capillary channel (right, superimposed to the solution of the elastica, marked in red): the deflection of the rod and the surface of the liquid have the same shape, see Section 4.

by the dynamical analysis presented in Section 3.1, so that, since bifurcation is shown to occur in our structures both in tension and compression, these can be used as two-way actuators for mechanical waves, where the axial force controls the speed of the waves traversing the structure. Therefore, the mechanical systems invented in the present article can immediately be generalized and employed to design complex mechanical systems exhibiting bifurcations in tension and compression, to be used, for instance, as systems with specially designed vibrational properties (a movie providing a simple illustration of the concepts exposed in this paper, together with a view of experimental results, is provided in the electronic supplementary material, see also <http://www.ing.unitn.it/dims/ssmg.php>).

2 A simple single-degree-of-freedom structure which buckles for tensile dead loading

The best way to understand how a structure can bifurcate under tensile dead loading is to consider the elementary single-degree-of-freedom structure shown in Fig. 2, where two rigid rods are connected through a ‘slider’ (a device which imposes the same rotation angle and axial displacement to the two connected pieces, but null shear transmission, leaving only the possibility of relative sliding).

Bifurcation load and equilibrium paths of this single-degree-of-freedom structure can be calculated by considering the bifurcation mode illustrated in Fig. 2 and defined by the rotation angle ϕ . The elongation of the system and the potential energy are respectively

$$\Delta = 2l \left(\frac{1}{\cos \phi} - 1 \right) \quad \text{and} \quad W(\phi) = \frac{1}{2}k\phi^2 - 2Fl \left(\frac{1}{\cos \phi} - 1 \right), \quad (1)$$

so that solutions of the equilibrium problem are

$$F = \frac{k \phi \cos^2 \phi}{2l \sin \phi}, \quad (2)$$

for $\phi \neq 0$, plus the trivial solution ($\phi = 0, \forall F$). Analysis of the second-order derivative of the strain energy reveals that the trivial solution is stable up to the critical load

$$F_{cr} = \frac{k}{2l}, \quad (3)$$

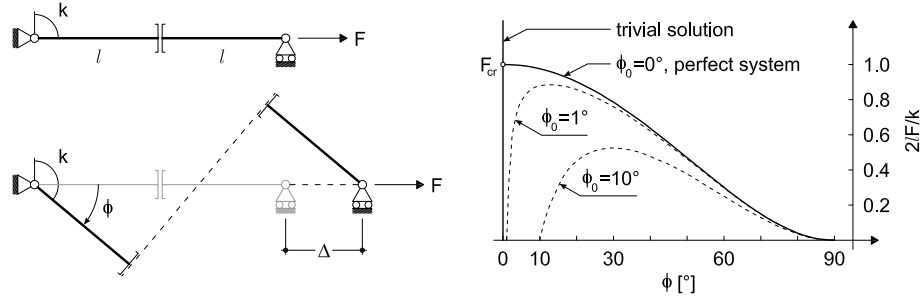


Fig. 2: Bifurcation of a single-degree-of-freedom elastic system under *tensile dead loading* (the rods of length l are rigid and jointed through a slider, a device allowing only for relative sliding between the two connected pieces). A rotational elastic spring of stiffness k , attached at the hinge on the left, provides the elastic stiffness. Note that the bifurcation is ‘purely geometrical’ and is related to the presence of the constraint at the middle of the beam which transmits rotation, but not shear (left). The bifurcation diagram, showing bifurcation and softening in tension is reported on the right. The rotation angle $\phi_0 = \{1^\circ, 10^\circ\}$ denotes an initial imperfection, in terms of an initial inclination of the two rods with respect to the horizontal direction.

while the nontrivial path, *evidencing softening*, is unstable. For an imperfect system, characterized by an initial inclination of the rods ϕ_0 , we obtain

$$W(\phi, \phi_0) = \frac{1}{2}k(\phi - \phi_0)^2 - 2Fl \left(\frac{1}{\cos \phi} - \frac{1}{\cos \phi_0} \right) \quad \text{and} \quad F = \frac{k(\phi - \phi_0) \cos^2 \phi}{2l \sin \phi}, \quad (4)$$

so that the force–rotation relation is obtained, which is reported as two dashed lines in Fig. 2 for $\phi_0 = 1^\circ$ and $\phi_0 = 10^\circ$.

The simple structure presented in Fig. 2, showing possibility of a bifurcation under dead load in tension and displaying an overall softening behaviour, can be realized in practice, as shown by the wooden model reported in Fig. 3.

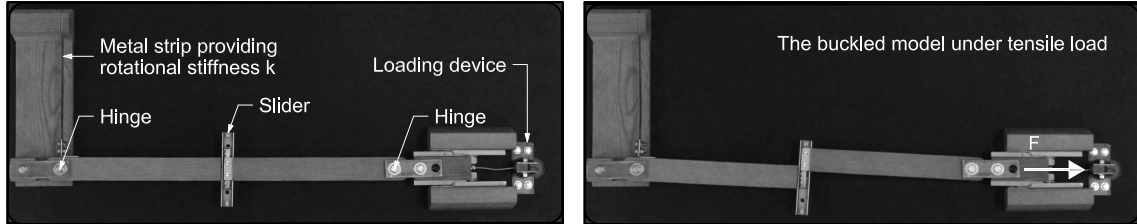


Fig. 3: A model of the single-degree-of-freedom elastic structure shown in Fig. 2 on the left (in which a metal strip reproduces the rotational spring and the load is given through hanging a load) displaying bifurcation for tensile dead loading (left: undeformed configuration; right: buckled configuration).

3 Vibrations, buckling and the elastica for a structure subject to tensile (and compressive) dead loading

In order to generalize the single-degree-of-freedom system model into an elastic structure, we consider two *inextensible* elastic rods clamped at one end and jointed through a slider, identical to that used to join the two rigid bars employed for the single-degree-of-freedom system (see the inset of Fig. 4). The two bars have bending stiffness B , length l^- (on the left) and l^+ (on the right) and are subject to a load F which may be tensile ($F > 0$) or compressive ($F < 0$).

3.1 The vibrations and critical loads

The differential equation governing the dynamics of an elastic rod subject to an axial force F (assumed positive if tensile) is

$$\frac{\partial^4 v(z, t)}{\partial z^4} - \frac{F}{B} \frac{\partial^2 v(z, t)}{\partial z^2} + \frac{\rho}{B} \frac{\partial^2 v(z, t)}{\partial t^2} = 0, \quad (5)$$

where ρ is the unit-length mass density of the rod and v the transversal displacement, so that time-harmonic motion is based on the separate-variable representation

$$v(z, t) = \tilde{v}(z) e^{-i\omega t}, \quad (6)$$

in which ω is the circular frequency, t is the time and $i = \sqrt{-1}$ is the imaginary unit.

A substitution of eqn (6) into eqn (5) yields the equation governing time-harmonic oscillations

$$\frac{d^4 \tilde{v}(z)}{dz^4} - \alpha^2 \text{sign}(F) \frac{d^2 \tilde{v}(z)}{dz^2} - \beta \tilde{v}(z) = 0, \quad (7)$$

where the function ‘sign’ (defined as $\text{sign}(\alpha) = |\alpha|/\alpha \forall \alpha \in \text{Re}$ and $\text{sign}(0) = 0$) has been used and

$$\alpha^2 = \frac{|F|}{B}, \quad \beta = \omega^2 \frac{\rho}{B}. \quad (8)$$

The general solution of eqn (7) is

$$\tilde{v}(z) = C_1 \cosh(\lambda_1 z) + C_2 \sinh(\lambda_1 z) + C_3 \cos(\lambda_2 z) + C_4 \sin(\lambda_2 z), \quad (9)$$

where

$$\lambda_1 = \sqrt{\frac{\sqrt{\alpha^4 + 4\beta} + \alpha^2 \text{sign}(F)}{2}}, \quad \lambda_2 = \sqrt{\frac{\sqrt{\alpha^4 + 4\beta} - \alpha^2 \text{sign}(F)}{2}}. \quad (10)$$

Eqn (9) holds both for the rod on the left (transversal displacement denoted with ‘-’) and on the right (transversal displacement denoted with ‘+’) shown in the inset of Fig. 4, so that the boundary conditions at the clamps impose

$$\tilde{v}^-(0) = \left. \frac{d\tilde{v}^-}{dz} \right|_{z=0} = 0, \quad \tilde{v}^+(l^+) = \left. \frac{d\tilde{v}^+}{dz} \right|_{z=l^+} = 0, \quad (11)$$

while at the slider we have the two conditions

$$\left. \frac{d^3 \tilde{v}^-}{dz^3} \right|_{z=l^-} = \left. \frac{d^3 \tilde{v}^+}{dz^3} \right|_{z=0} = 0, \quad (12)$$

expressing the vanishing of the shear force. The imposition of the six conditions (11)–(12) provides the constants $C_{2,3,4}^\pm$ as functions of the constants C_1^\pm , so that the continuity of the rotation at the slider

$$\left. \frac{d\tilde{v}^-}{dz} \right|_{z=l^-} = \left. \frac{d\tilde{v}^+}{dz} \right|_{z=0} \quad (13)$$

and the equilibrium of the slider

$$\left. \frac{d^2 \tilde{v}^-}{dz^2} \right|_{z=l^-} - \alpha^2 \text{sign}(F) \tilde{v}^-(l^-) = \left. \frac{d^2 \tilde{v}^+}{dz^2} \right|_{z=0} - \alpha^2 \text{sign}(F) \tilde{v}^+(0), \quad (14)$$

yields finally a linear homogeneous system (with unknowns C_1^- and C_1^+), whose determinant has to be set equal to zero, to obtain the frequency equation, function of α^2 , ω and $\text{sign}(F)$.

The circular frequency ω (normalized through multiplication by $\sqrt{\rho l^4/B}$) versus the axial force (normalized through multiplication by $4l^2/(B\pi^2)$) is reported in Fig. 4, where the first four branches are shown for a system of two rods of equal length. In this figure the gray zones

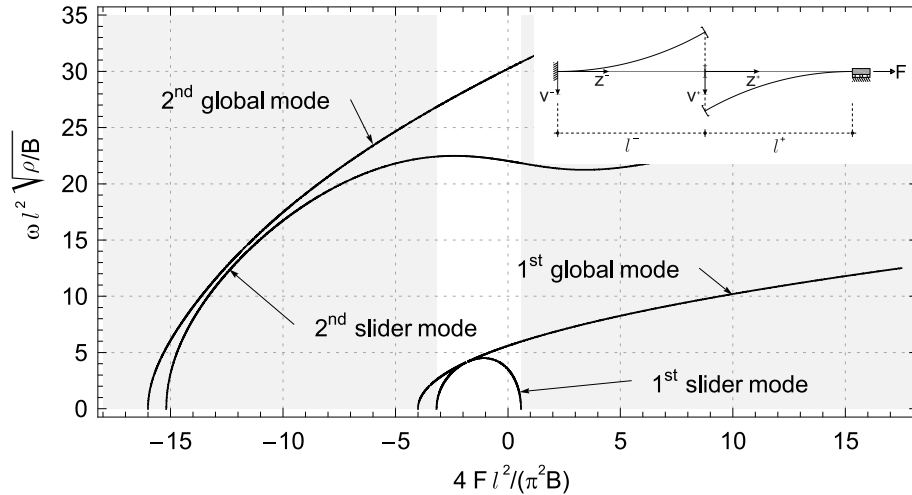


Fig. 4: Dimensionless circular frequency ω for the structure shown in the inset (in the particular case of rods of equal length, l) as a function of the dimensionless applied load F . Note that solutions in the gray region cannot be achieved, since the rods cannot remain straight for axial forces external to the bifurcation range of loads (shown as a white zone).

represent situations that cannot be achieved, in the sense that the axial force falls outside the interval where the straight configuration of the system is feasible (in other words, for axial loads external to the interval of first bifurcations in tension and compression, the straight configuration cannot be maintained).

The branches shown in Fig. 4 intersect the horizontal axis in correspondence of the bifurcation loads of the system, namely, $4F_{cr}l^2/(\pi^2B) = -16, -15.19, -4, -3.17, +0.58$, so that there is one critical load in tension (the corresponding branch is labeled ‘1st slider mode’ in Fig. 4), and infinitely many bifurcation loads in compression, the first three are reported in Fig. 4 (bifurcations corresponding to the label ‘global mode’ do not involve relative displacement across the slider).

Beside the possibility of bifurcation in tension, an interesting and novel effect related to the presence of the slider is that a tensile (compressive) axial force yields a decrease (increase) of the frequency of the system, while an opposite effect is achieved when ‘global modes’ are activated.

Quasi-static solutions of the system and related bifurcations can be obtained in the limit $\omega \rightarrow 0$ of the *frequency equation*, which yields

$$\begin{cases} \tanh(\alpha l^-) \cosh(\alpha l^+) + \sinh(\alpha l^+) [1 - (l^+ + l^-) \alpha \tanh(\alpha l^-)] = 0, & \text{for } F > 0, \\ \tan(\alpha l^-) \cos(\alpha l^+) + \sin(\alpha l^+) [1 + (l^+ + l^-) \alpha \tan(\alpha l^-)] = 0, & \text{for } F < 0. \end{cases} \quad (15)$$

In the particular case of rods of equal length l , eqns (15) simplify to

$$\begin{cases} \sinh(\alpha l) [1 - \alpha l \tanh(\alpha l)] = 0, & \text{for } F > 0, \\ \sin(\alpha l) [1 + \alpha l \tan(\alpha l)] = 0, & \text{for } F < 0. \end{cases} \quad (16)$$

Eqns (16) show clearly that *there is only one bifurcation load in tension* (branch labeled ‘1st slider mode’ in Fig. 4), but there are ∞^2 bifurcation loads in compression (the first three branches are reported in Fig. 4). In compression, the bifurcation condition $\sin(\alpha l) = 0$, providing ∞^1 solutions, yields the critical loads of a doubly clamped beam of length $2l$ and defines what we have labeled ‘global modes’ in Fig. 4.

Bifurcation loads, normalized through multiplication by $(l^+ + l^-)^2/(\pi^2B)$, are reported in Fig. 5 as functions of the ratio l^+/l^- between the lengths of the two rods. Note that the graph is plotted in a semi-logarithmic scale, which enforces symmetry about the vertical axis. In the graph, the first two buckling loads in compression are reported: the first corresponds to a mode involving sliding, while the second does not involve any sliding (and when $l^+ = l^-$ corresponds to the first mode of a doubly clamped rod of length $2l$). Used as an optimization parameter, $l^+ = l^-$ corresponds to the lower bifurcation load in tension (+0.58), near five times smaller (in absolute value) that the buckling load in compression (−3.17).

3.2 The elastica

The determination of the non-trivial configurations at large deflections of the mechanical system requires a careful use of Euler’s elastica. It is instrumental to employ the reference systems shown in Fig. 6 and impose one kinematic compatibility condition and three equilibrium conditions. These are as follows.

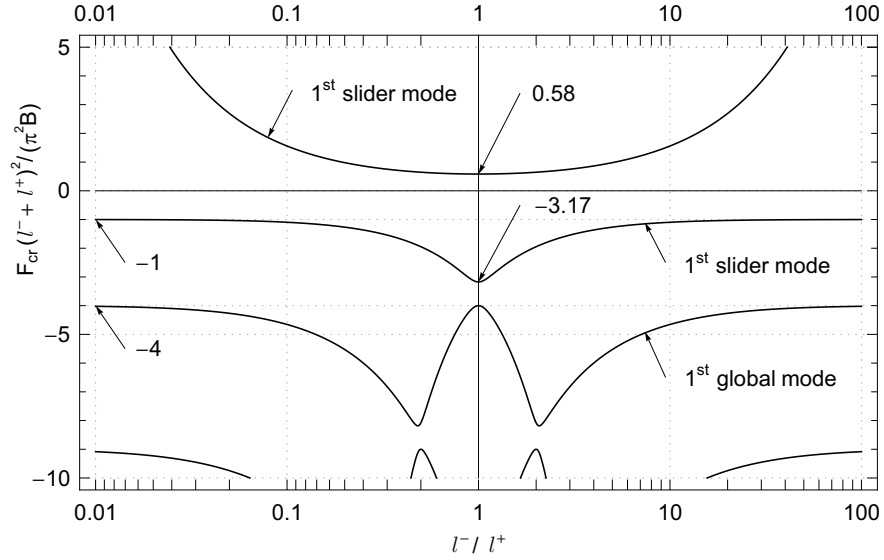


Fig. 5: Dimensionless critical loads F_{cr} as a function of the ratio between the lengths of the rods, l^+/l^- . The dimensionless axial forces for bifurcation in tension and those corresponding to the first two modes in compression are reported.

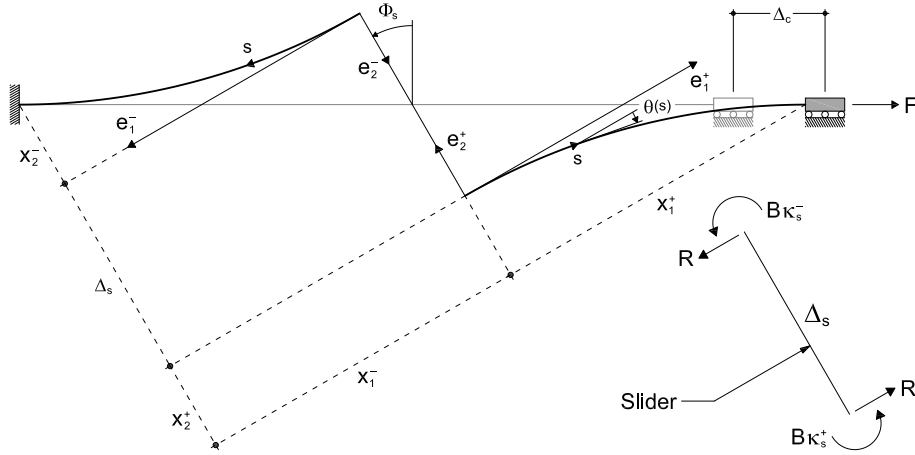


Fig. 6: Sketch of the problem of the elastica under tensile axial load F . Note the reference systems employed in the analysis and note that the moments on the slider have been reported positive and the curvature results to be negative.

- The kinematic compatibility condition can be directly obtained from Fig. 6 noting that the jump in displacement across the slider (measured orthogonally to the line of the elastica), Δ_s , can be related to the angle of rotation of the slider Φ_s , a condition that assuming the local reference systems shown in Fig. 6 becomes

$$[x_1^-(l^-) + x_1^+(l^+)] \tan \Phi_s + x_2^-(l^-) + x_2^+(l^+) + \Delta_s = 0, \quad (17)$$

where $x_1(s)$ and $x_2(s)$ are the coordinates of the elastica and the index $- (+)$ denotes that the quantities are referred to the rod on the left (on the right). Note that Φ_s is assumed positive when anticlockwise and Δ_s is not restricted in sign (negative in the case of Fig. 6).

- Since the slider can only transmit a moment and a force R orthogonal to it, equilibrium requires that (see the inset in Fig. 6)

$$R = \frac{F}{\cos \Phi_s}, \quad (18)$$

where F is the axial force providing the load to the rod, assumed positive (negative) when tensile (compressive), so that since $\Phi_s \in [-\pi/2, \pi/2]$, R is positive (negative) for tensile (compressive) load. Note that with the above definitions we have

$$\theta^+(0) = \theta^-(0) = 0, \quad \theta^+(l^+) = \theta^-(l^-) = -\Phi_s. \quad (19)$$

- Equilibrium of the slider requires that

$$\kappa_s^- + \kappa_s^+ = \frac{R}{B} \Delta_s, \quad (20)$$

where B is the bending stiffness of the rod and κ_s^\pm is the curvature on the left ($-$) or on the right ($+$) of the slider. Note that B is always positive, but R , κ_s^\pm and Δ_s can take any sign.

- For both rods (left and right) rotational equilibrium of the element of rod singled out at curvilinear coordinate s requires

$$\frac{d^2\theta}{ds^2} - \frac{R}{B} \sin \theta = 0, \quad (21)$$

where θ is the rotation of the normal at each point of the elastica, assumed positive when anticlockwise, with added the superscript $- (+)$ to denote the rod on the left (on the right).

Eqn (21) is usually (see for instance Love, 1927, his eqn (8) at Sect. 262) written with a sign ‘+’ replacing the sign ‘-’ and R is assumed positive when compressive; the same equation describes the motion of a simple pendulum (see for instance Temme, 1996). The ‘+’ sign originates from the fact that the elastica has been analyzed until now only for deformations originating from compressive loads. However, an equation with the ‘-’ sign and with R/B replaced by the ratio between unit weight density and surface tension of a fluid –thus equal to eqn (21)– determines *the shape of the capillary curve of a liquid* (Lamb, 1928), which therefore results to be identical to the deflection of a rod under tensile load.

In the following we derive equations holding along both rods ‘+’ and ‘-’, so that these indices will be dropped for simplicity. Multiplication of eqn (21) by $d\theta/ds$ and integration from 0 to s yields

$$\left(\frac{d\theta}{ds}\right)^2 = -2\tilde{\alpha}^2 \text{sign}(R) \cos \theta + 2\tilde{\alpha}^2 \left(\frac{2}{k^2} - 1\right), \quad (22)$$

where, using the Heaviside step function H , we have

$$\tilde{\alpha}^2 = \frac{|R|}{B} \quad \text{and} \quad k^2 = \left(\frac{\kappa_s^2}{4\tilde{\alpha}^2} + H(R) \right)^{-1}. \quad (23)$$

Eqn (22) can be re-written as

$$\left(\frac{d\theta}{ds} \right)^2 = \frac{4\tilde{\alpha}^2}{k^2} \left[1 - k^2 \sin^2 \left(\frac{\theta}{2} + \frac{\pi}{2} H(R) \right) \right], \quad (24)$$

so that the change of variable $u = s\tilde{\alpha}/k$ yields

$$\frac{d\theta}{du} = \pm 2 \sqrt{1 - k^2 \sin^2 \left(\frac{\theta}{2} + \frac{\pi}{2} H(R) \right)}. \quad (25)$$

The analysis will be restricted for simplicity to the case ‘+’ in the following. At $u = 0$ it is $\theta = 0$, so that eqn (25) gives the solution

$$\theta = 2 \operatorname{am} [u + KH(R), k] - \pi H(R) \quad \text{and} \quad \frac{d\theta}{ds} = \frac{2}{k} \tilde{\alpha} \operatorname{dn} [u + KH(R), k], \quad (26)$$

where am and dn are respectively the Jacobi elliptic functions amplitude and delta-amplitude and K is the complete elliptic integral of the first kind (Byrd and Friedman, 1971). Since in the local reference system we have $dx_1/ds = \cos \theta$ and $dx_2/ds = \sin \theta$, an integration gives the coordinates x_1 and x_2 of the elastica expressed in terms of u ,

$$\left. \begin{aligned} x_1 &= \frac{1}{k\tilde{\alpha}} \left[(2 - k^2)u - 2\operatorname{E}[\operatorname{am}[u, k], k] + 2k^2 \operatorname{sn}[u, k] \operatorname{cn}[u, k] \right] \\ x_2 &= \frac{2}{k\tilde{\alpha}} \sqrt{1 - k^2} \left(\frac{1 - \operatorname{dn}[u, k]}{\operatorname{dn}[u, k]} \right) \end{aligned} \right\} \quad \text{for } R > 0, \quad (27)$$

for tensile axial loads, while for compressive axial loads

$$\left. \begin{aligned} x_1 &= \frac{1}{k\tilde{\alpha}} \left[(k^2 - 2)u + 2\operatorname{E}[\operatorname{am}[u, k], k] \right] \\ x_2 &= \frac{2}{k\tilde{\alpha}} (1 - \operatorname{dn}[u, k]) \end{aligned} \right\} \quad \text{for } R < 0, \quad (28)$$

in which the constants of integration are chosen so that x_1 and x_2 vanish at $s = 0$. In eqns (27)–(28) sn and cn are respectively the Jacobi elliptic functions sine-amplitude and cosine-amplitude and E is the incomplete elliptic integral of the second kind (Byrd and Friedman, 1971).

Eqns (28) differ from eqns (16) reported by Love (1927, his Section 263) only in a translation of the coordinate x_2 , while eqns (27), holding for tensile axial force, are new.

Finally, with reference to Fig. 6, we note that the horizontal displacement Δ_c of the right clamp can be written in the form

$$\Delta_c = \frac{x_1^-(l^-) + x_1^+(l^+)}{\cos \Phi_s} - (l^+ + l^-). \quad (29)$$

To find the axial load F as a function of the slider rotation Φ_s , or as a function of the end displacement Δ_c , we have now to proceed as follows:

- values for κ_s^- and κ_s^+ are fixed (as a function of the selected mode, for instance, $\kappa_s^- = \kappa_s^+$, to analyze the bifurcation mode in tension);
- k can be expressed using eqn (23) as a function of $\tilde{\alpha}$;
- the equations for the coordinates of the elastica, eqn (27) for tensile load, or eqn (28) for compressive load, and eqn (26)₁, evaluated at l^- and l^+ , become functions of only $\tilde{\alpha}$;
- eqns (19) and (20) provide Φ_s and Δ_s , so that eqn (17) becomes a nonlinear equation in the variable $\tilde{\alpha}$, which can be numerically solved (we have used the function FindRoot of Mathematica[®] 6.0);
- when $\tilde{\alpha}$ is known, R and F can be obtained from eqns (23) and (18);
- finally, Φ_s and Δ_c are calculated using eqns (19) and (29).

Results are shown in Fig. 7 for tensile loads and in Fig. 8 for compressive loads, in terms of dimensionless axial load $4Fl^2/(B\pi^2)$ versus slider rotation Φ_s (on the left) and dimensionless end displacement $\Delta_c/(2l)$ (on the right).

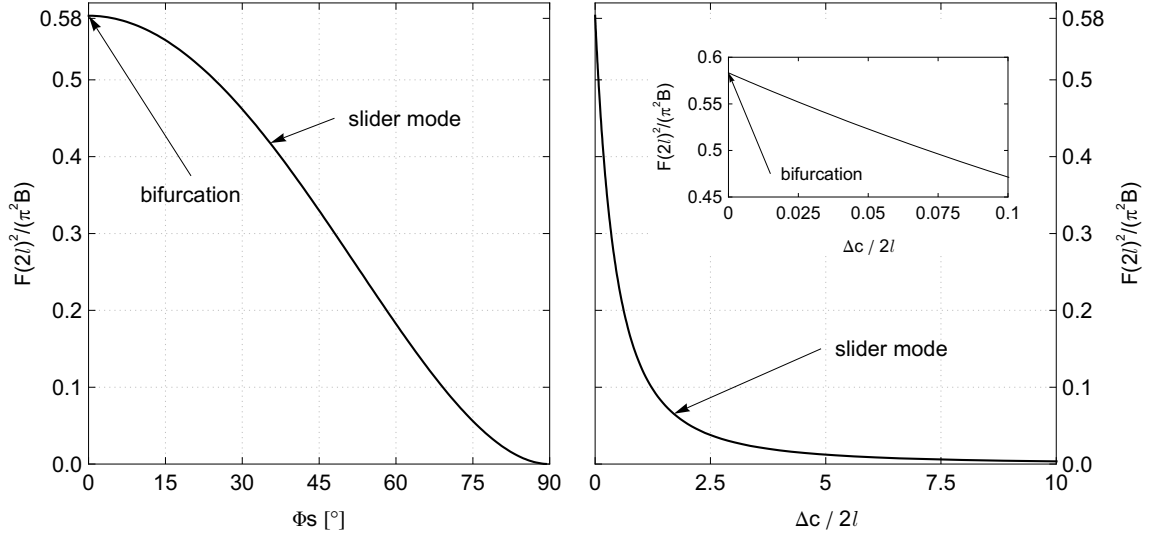


Fig. 7: Bifurcation of the structure sketched in Fig. 6 under tensile load. Dimensionless axial load F versus slider rotation (versus dimensionless end displacement) is shown on the left (on the right).

Note that, while there is only one bifurcation in tension, there are infinite bifurcations in compression, so that we have limited results to the initial three modes in compression. Two of these modes involve slider rotation (labeled ‘slider mode’), while an intermediate mode (labeled ‘global mode’) does not.

The load/displacement curve shown in Fig. 7 on the left is plotted until extremely large displacements, namely, $\Delta_c = 20l$ (a detail at moderate displacement is reported in the inset). It displays a *descending, in other words softening and unstable, postcritical behaviour*, which

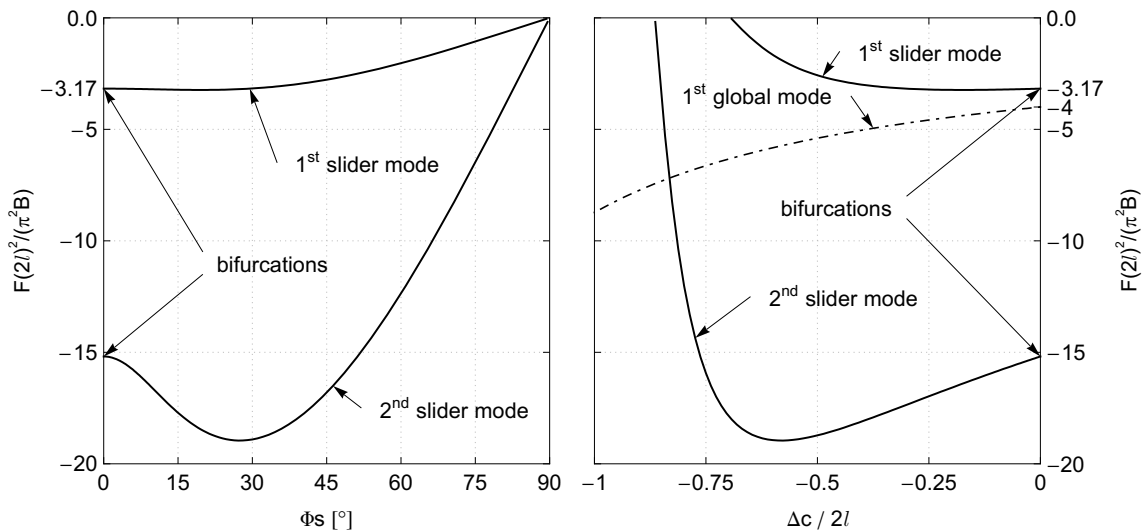


Fig. 8: Bifurcation of the structure sketched in Fig. 6 under compressive load. Dimensionless axial load F versus slider rotation (versus dimensionless end displacement) is shown on the left (on the right).

contrasts with the usual postcritical of the elastica under various end conditions, in which the load rises with displacement. In compression, the post-critical behaviour evidences another novel behaviour, so that the first and the second slider modes present an initial part where the load/displacement rises, followed by a softening behaviour. Finally, it is important to note that the curves load versus Φ_s in Figs. 7 and 8, both *for tension and compression intersect each other at null loading at the extreme rotation $\Phi_s = 90^\circ$* , which means that two unloaded configurations (in addition to the initial configuration) exist. These peculiarities, never observed before in simple elastic structures, are all related to the presence of the slider.

Deformed elastic lines are reported in Fig. 9, both for tension and compression, the latter corresponding to the first three slider modes (the global mode is not reported since it corresponds to the first mode of a doubly-clamped rod).

4 Experimental

The structure sketched in Fig. 6 has been realized with two carbon steel AISI 1095 strips (250 mm \times 25 mm \times 1 mm; Young modulus 200 GPa) and the slider with two linear bearings (type Easy Rail SN22-80-500-610, purchased from Rollon[®]), commonly used in machine design applications, see the inset of Fig. 10. The slider is certified by the producer to have a low friction coefficient, equal to 0.01. Tensile force on the structure has been provided by imposing displacement with a load frame ELE Tritest 50 (ELE International Ltd), the load measured with a load cell Gefran OC-K2D-C3 (Gefran Spa), and the displacement with a potentiometric transducer Gefran PY-2-F-100 (Gefran Spa). Data have been acquired with system NI CompactDAQ, interfaced with Labview 8.5.1 (National Instruments). Photos have been taken with a Nikon D200 digital camera, equipped with a AF-S micro Nikkor lens (105 mm 1:2.8G ED)

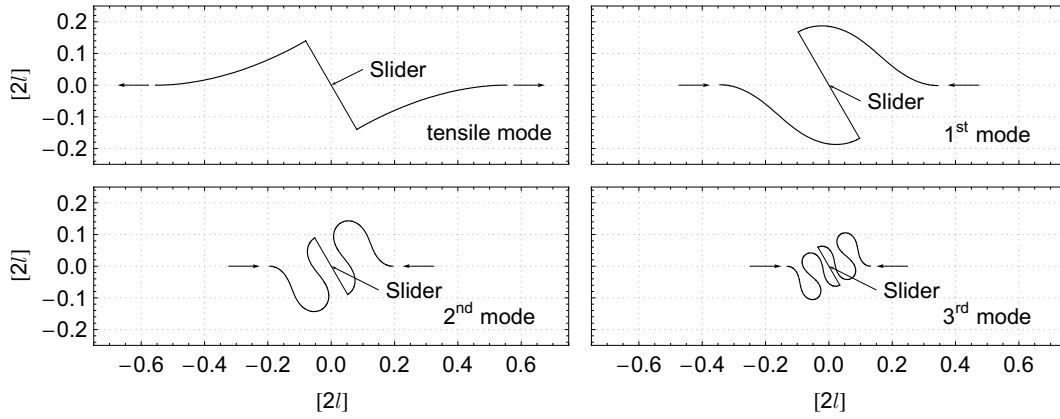


Fig. 9: Deflections (the scale of the axes is $2l$) of the structure shown in Fig. 6 (with rods of equal length) at a slider rotation of 30° in tension (upper part, on the left) and compression (first 3 slider modes are reported, whereas the global mode has not been reported).

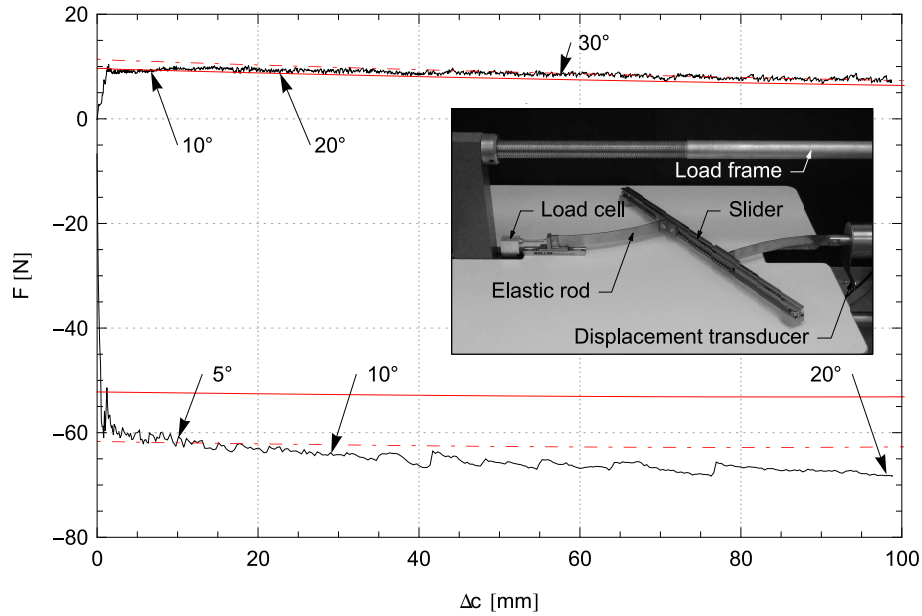


Fig. 10: Load versus end displacement for the model representing the structure sketched in Fig. 6 recorded during tensile (positive F) and compressive (negative F) tests. The red curves are the theoretical predictions (the dashed line is obtained keeping into account the effective values of the lengths of the rods, 10% smaller than the values measured from the clamps to the middle of the slider). The values ' 5° ', ' 10° ', ' 20° ' and ' 30° ' denote the inclination of the slider in degrees reached during the test. A photo of the experimental setup during the postcritical behaviour in tension is reported in the inset.

and movies with a Sony Handycam HDR-XR550. Tensile and compressive tests have been run at a velocity of 2.5 mm/s.

Photos taken at different slider rotations (and thus load levels) are shown in Fig. 11 for tension ($\Phi_s = 0^\circ, 10^\circ, 20^\circ, 30^\circ$) and in Fig. 12 for compression ($\Phi_s = 0^\circ, 5^\circ, 10^\circ, 20^\circ$). A comparison between theoretical predictions and experiments is reported in the lower parts of the figures where photos are superimposed to the line of the elastica, shown in red and plotted using eqn (27) for tensile load and eqn (28) for compression.

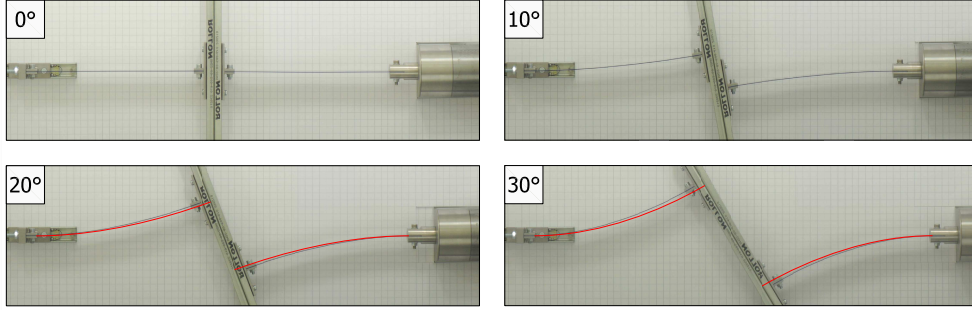


Fig. 11: Photos of the model representing the structure sketched in Fig. 6 and loaded in tension at different values of slider rotation $\Phi_s = 0^\circ, 10^\circ$, (upper part) $20^\circ, 30^\circ$ (center). The elastica calculated with eqn (27) is superimposed on the photos at $20^\circ, 30^\circ$ in the lower part. The side of the grid marked on the paper is 10 mm.

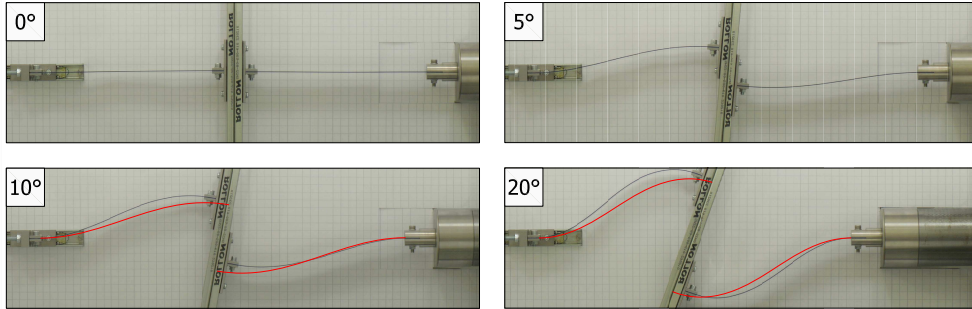


Fig. 12: Photos of the model representing the structure sketched in Fig. 6 and loaded in compression at different values of slider rotation $\Phi_s = 0^\circ, 5^\circ$, (upper part) $10^\circ, 20^\circ$ (center). The elastica calculated with eqn (27) is superimposed on the photos at $10^\circ, 20^\circ$ in the lower part. The side of the grid marked on the paper is 10 mm.

These experiments show clearly the existence of the bifurcation in tension and provide an excellent comparison with theoretical results obtained through integration of the elastica both in tension and in compression. A further quantitative comparison between theoretical results and experiments is provided in Fig. 10, where the axial load in the structure (positive for tension and negative for compression) is plotted versus the end displacement Δ_c . The experimental result is compared to theoretical results (marked red) expressed by eqn (29), used in the way detailed at the end of Section 3.2.

The theoretical result marked in red with continuous curve has been calculated assuming an initial length of the rods (25 cm) measured from the end of the clamps to the middle of the slider. However, the slider and the junctions to the metal strips are 58 mm thick, so that the

system is stiffer in reality. Therefore, we have plotted dashed the theoretical results obtained employing an ‘effective’ initial length of the rods reduced of 10% (so that the effective length of the system has been taken equal to 45 cm). The experimental curve evidences oscillations of ± 1 N for tensile loads and ± 5 N for compressive loads. These oscillations are due to friction within the slider, so that it is obvious that the oscillations are higher in compression than in tension, since in the former case the load is higher. Except for these oscillations, the friction (which is very low) has been found not to influence the tests.

The fact that experimentally the bifurcations initiate before the theoretical values are attained represents the well-known effect of imperfections, so that we may conclude that the agreement between theory and experiments is excellent.

To provide experimental evidence to the fact that the elastica in tension corresponds to the shape of the free surface of a liquid in a capillary channel, we note that a meniscus in a capillary channel satisfies (by symmetry) a null-rotation condition at the centre of the channel, so that it corresponds to a clamped edge of a rod. If the tangent to the meniscus at the contact with the channel wall is taken to correspond to the rotation of the non-clamped edge of the rod and the width of the channel is calculated employing the elastica, the elastic deflection of the rod scales with the free surface of the liquid. Therefore, we have performed an experiment in which we have taken a photo (with a Nikon SMZ800 stereo-zoom microscope equipped with Nikon Plan Apo 0.5x objective and a Nikon DD-FI1 high definition color camera head) of a water meniscus in a polycarbonate channel. We have proceeded as follows. First, we have observed that the contact angle between a water surface in air and polycarbonate (at a temperature of 20°C) is 70°. Second, we have taken a photo of the meniscus formed in a polycarbonate ‘V-shaped’ channel with walls inclined at 10° with the vertical, so that the angle between the horizontal direction and the free surface results to be 30° and the distance between the walls results 6 mm. This photo has been compared with a photo taken (with a Nikon D200 digital camera, and shown in Fig. 11 on the right) during buckling in tension when the elastic rods form the same angle of 30°. The result is shown in Fig. 1, together with the theoretical solution shown red.

Conclusions

We have theoretically proven and fully experimentally confirmed that elastic structures can be designed and practically realized in which bifurcation can occur with tensile dead loading. In these structures no parts subject to compression are present. The finding is directly linked to the presence of a junction allowing only for relative sliding between two parts of the mechanical system. Our findings open completely new and unexpected perspectives, related for instance to the control of the propagation of mechanical waves and to the understanding of certain failure modes in material elements.

Acknowledgments

The authors gratefully acknowledge financial support from PRIN grant No. 2007YZ3B24.

References

- [1] Bigoni, D., Gei, M. and Movchan, A.B. (2008) Dynamics of a prestressed stiff layer on an elastic half space: filtering and band gap characteristics of periodic structural models derived from long-wave asymptotics. *J. Mech. Phys. Solids*, 56, 2494-2520.
- [2] Byrd, P.F and Friedman, M.D. (1971) *Handbook of elliptic integrals for engineers and scientists*. Springer-Verlag.
- [3] Gajewski, A. and Palej, R. (1974) Stability and shape optimization of an elastically clamped bar under tension (in Polish). *Rozprawy Inzynierskie - Engineering Transactions*, 22, 265-279.
- [4] Gei, M., Movchan, A.B. and Bigoni, D. (2009) Band-gap shift and defect-induced annihilation in prestressed elastic structures. *J. Appl. Phys.*, 105, 063507.
- [5] Lamb, H. (1928) *Statics*. Cambridge University Press.
- [6] Love, A.E.H. (1927) *A treatise on the mathematical theory of elasticity*. Cambridge University Press.
- [7] Temme, N.M. (1996) *Special functions*. John Wiley and Sons, New York.
- [8] Timoshenko, S.P. and Gere, J.M. (1961) *Theory of elastic stability*. McGraw-Hill, New York.
- [9] Ziegler, H. (1977) *Principles of structural stability*. Birkäuser Verlag.
- [10] Zyczkowski, M. (1991) *Strength of structural elements*. Elsevier.